Supporting Information

Multi-scale structure optimization of boron-doped hard carbon nanospheres boosting plateau capacity for high performance sodium ion battery

Dongyang Wu,[a] Fei Sun,*[a] Zhibin Qu,[a] Hua Wang,[a] Zhuojia Lou,[a] Bin Wu,[b] and Guangbo Zhao*[a]

[a] School of Energy Science and Engineering, Harbin Institute of Technology, Harbin, 150001, China

[b] School of Chemistry and Chemical Engineering, Shanghai University of Engineering Science, Shanghai 201620, China

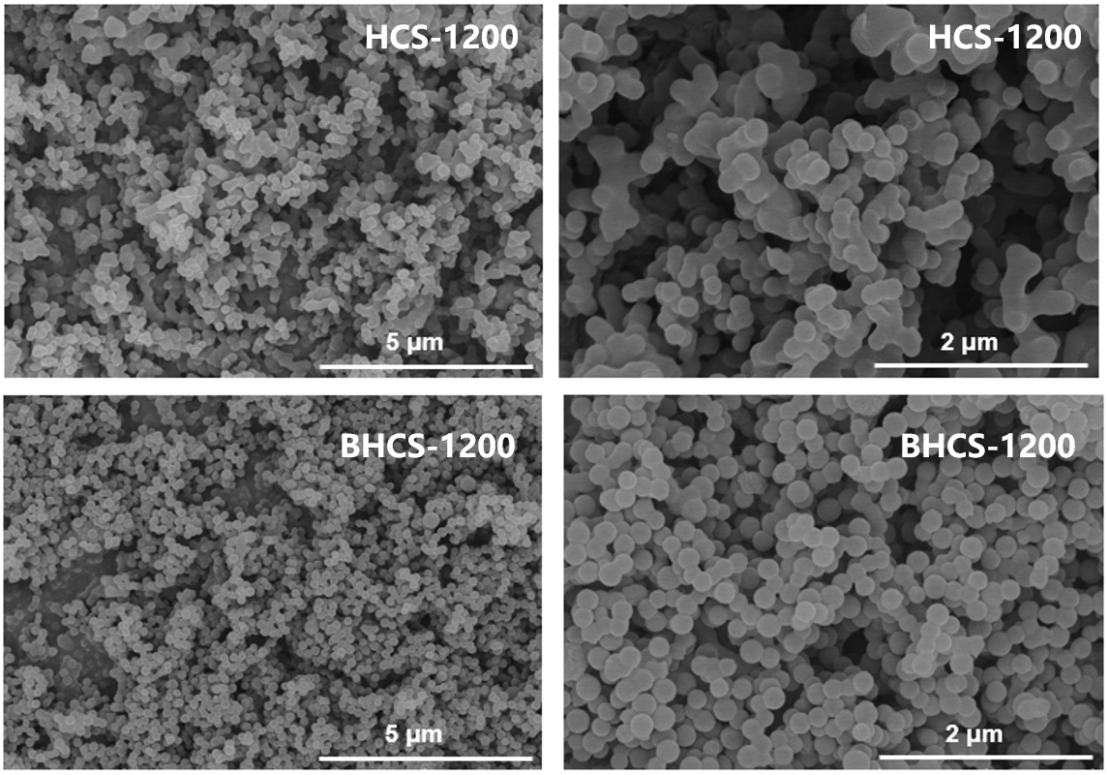

Figure S1. SEM images of HCS-1200 and BHCS-1200 at different magnification rates.

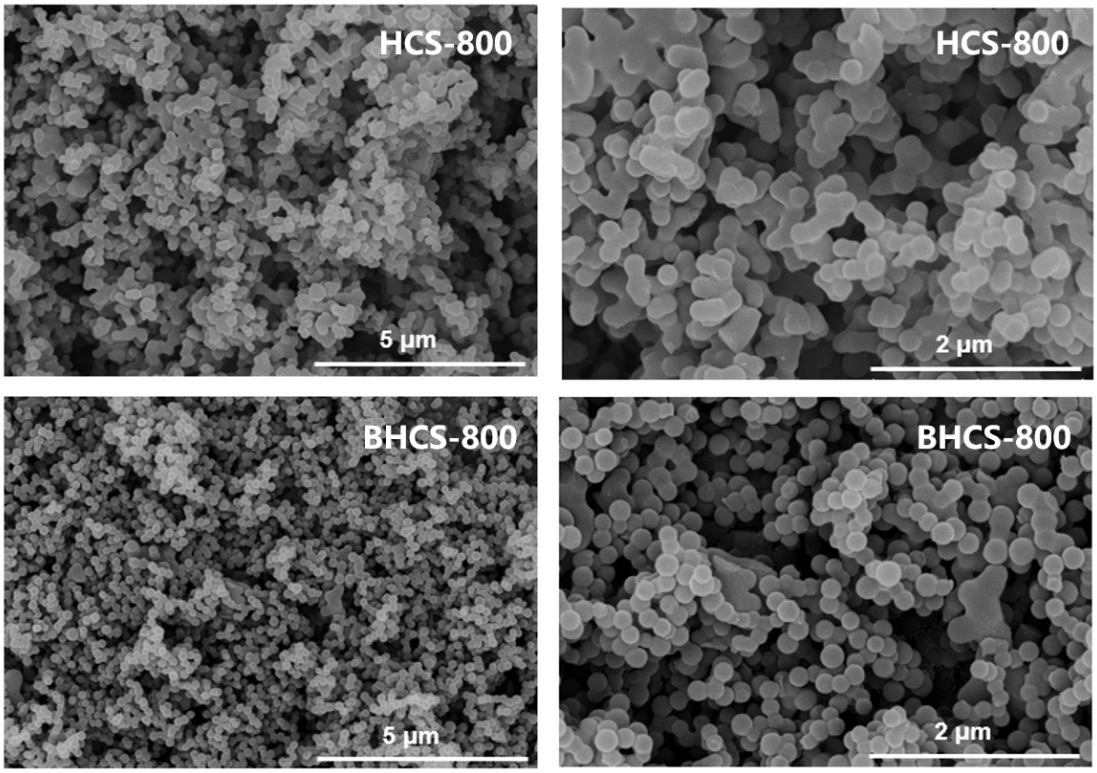

Figure S2. SEM images of HCS-800 and BHCS-800 at different magnification rates.

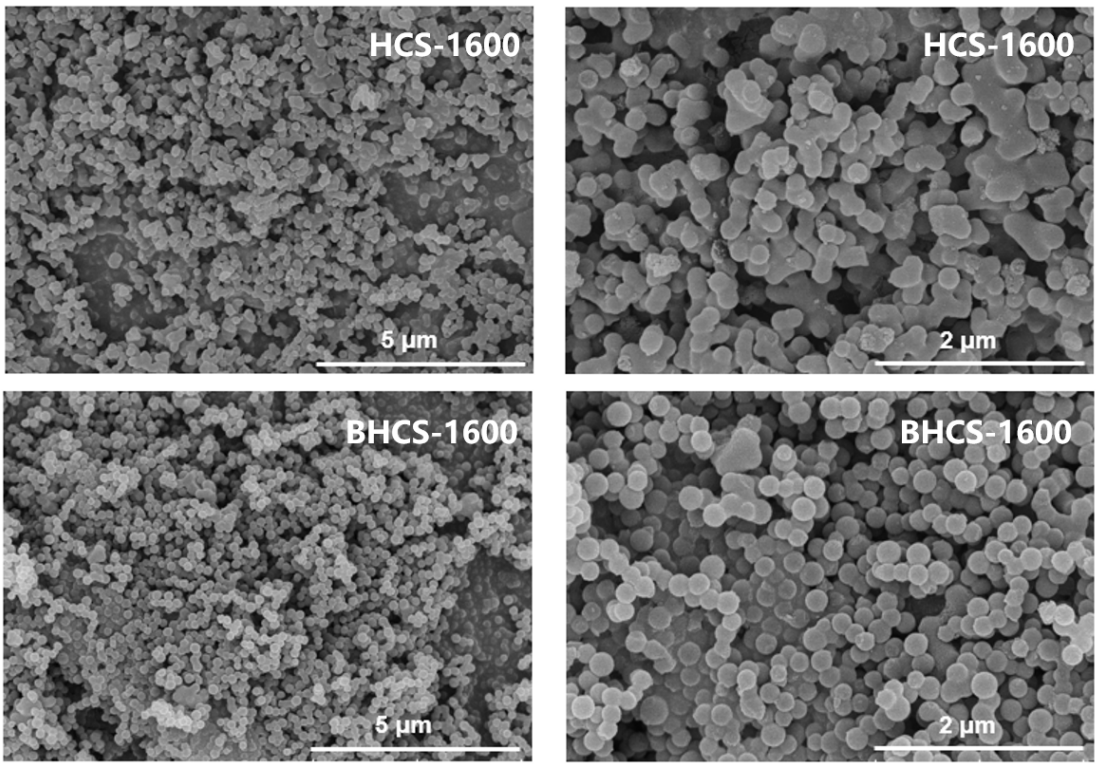

Figure S3. SEM images of HCS-1600 and BHCS-1600 at different magnification rates.

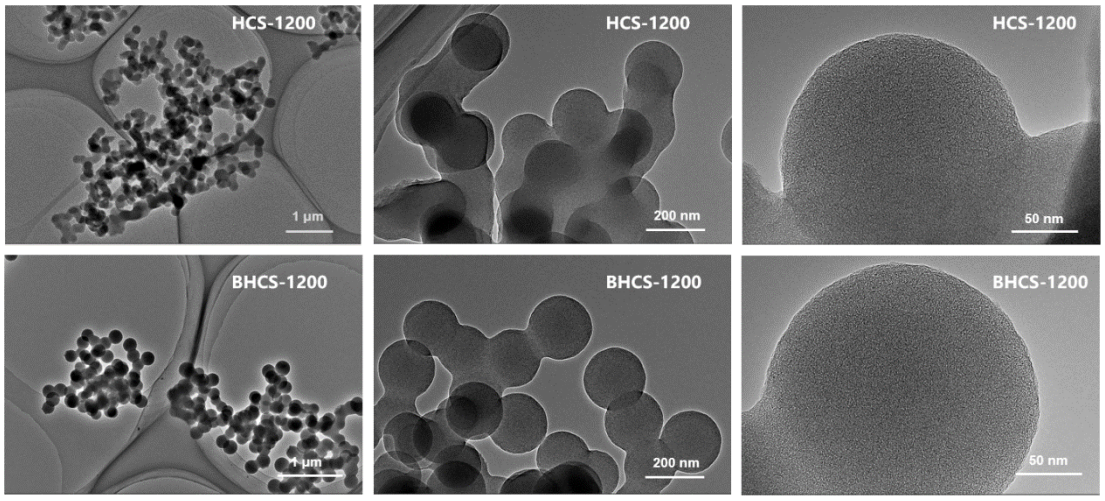

Figure S4. TEM and HRTEM images of HCS-1200 and BHCS-1200 at different magnification rates.

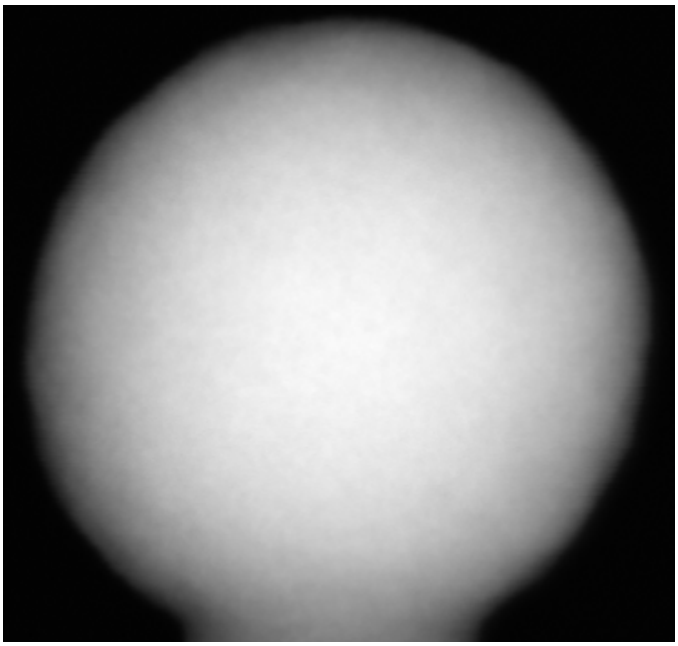

Figure S5. Electron image of BHCS-1200.

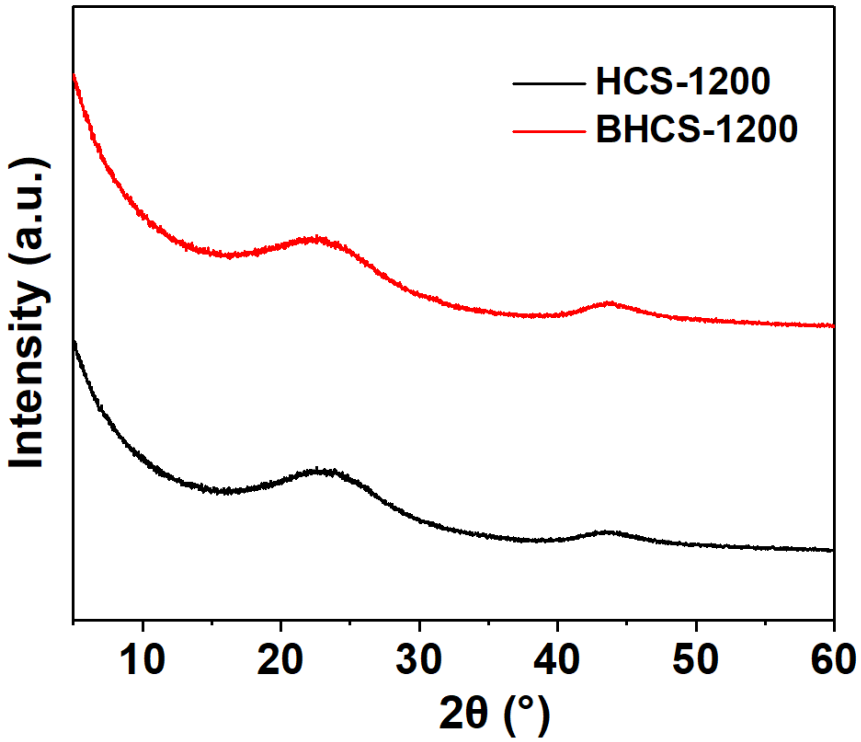

Figure S6. XRD patterns of HCS-1200 and BHCS-1200.

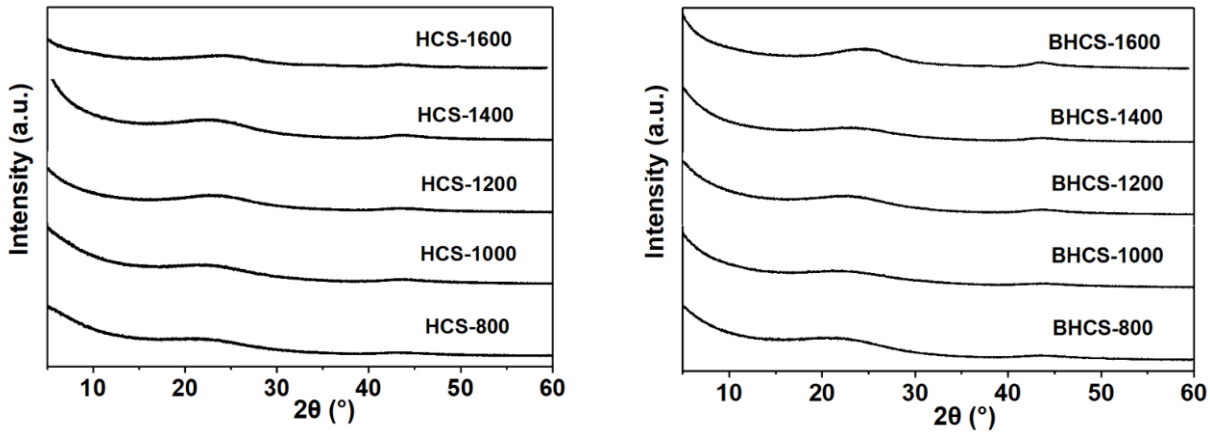

Figure S7. XRD patterns of HCS-*x* and BHCS-*x*.

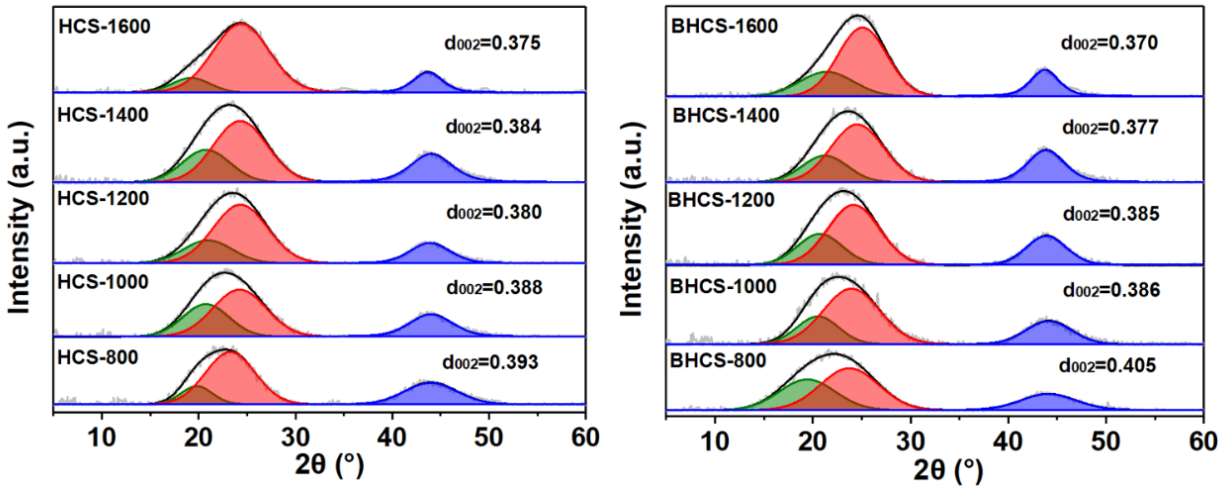

Figure S8. Deconvoluted XRD patterns of HCS-*x* and BHCS-*x* with d_{002} parameters.

Table S1. Structural parameters of microcrystals from XRD patterns for HCS-*x* and BHCS-*x*.

Samples	d_{002} (nm)	L_a (nm)	L_c (nm)
HCS-800	0.393	2.766	1.419
BHCS-800	0.405	2.648	1.158
HCS-1000	0.388	3.329	1.305
BHCS-1000	0.386	3.171	1.258

HCS-1200	0.380	3.592	1.249
BHCS-1200	0.385	3.652	1.349
HCS-1400	0.384	3.467	1.273
BHCS-1400	0.377	3.923	1.317
HCS-1600	0.375	4.934	1.222
BHCS-1600	0.370	5.142	1.329

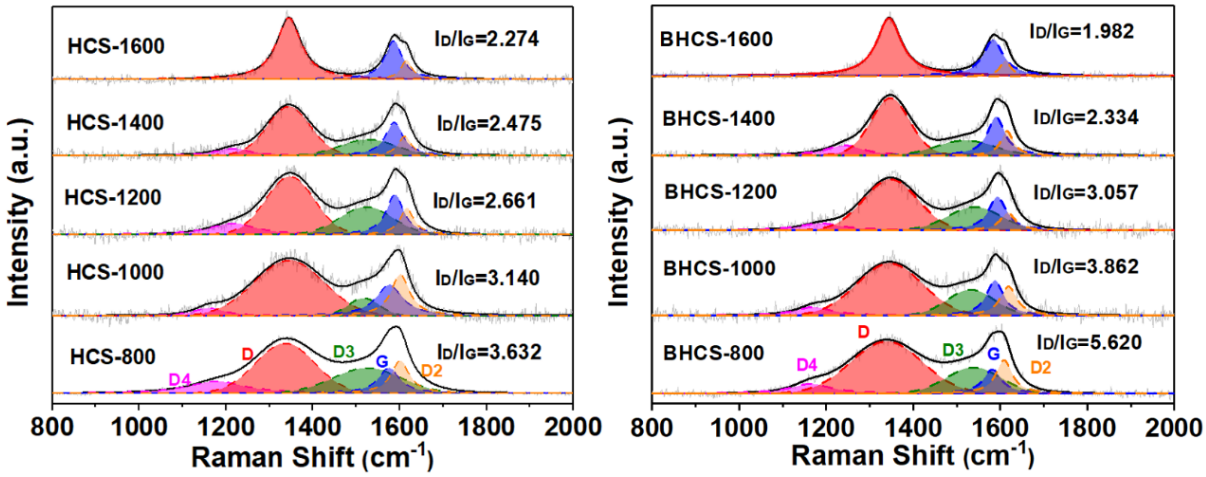

Figure S9. Deconvoluted Raman spectras of HCS-*x* and BHCS-*x* with I_D / I_G parameters.

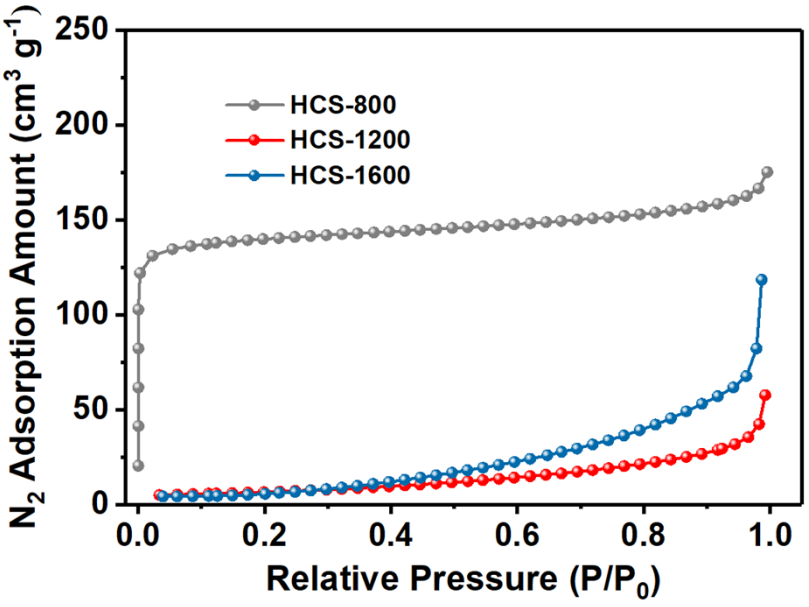

Figure S10. N_2 adsorption isotherms of HCS-800, HCS-1200 and HCS-1600.

Table S2. Content of boron doping configurations from XPS spectrum for BHCS-800, BHCS-1200 and BHCS-1600.

Samples	BC_3 (%)	BC_2O (%)	BCO_2 (%)	B_4C (%)
BHCS-800	19.49	31.47	49.04	
BHCS-1200	44.13	28.77	27.10	
BHCS-1600	42.13	17.61	16.48	24.08

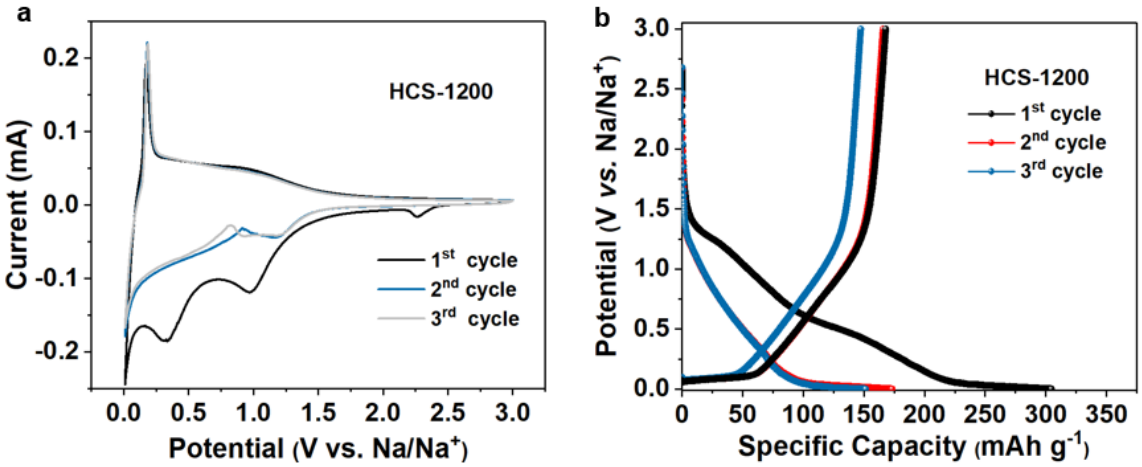

Figure S11. Na^+ anodic performances of HCS-1200 using coin-type cells in 1 M $NaPF_6$ electrolyte with mass loading of 0.8-1.2 mg cm^{-2}. **(**a) CV curves of HCS-1200 at the scan rate of 0.2 mV s^{-1}. **(**b) Initial three discharge–charge curves of HCS-1200 at the current density of 0.03 A g^{-1}.

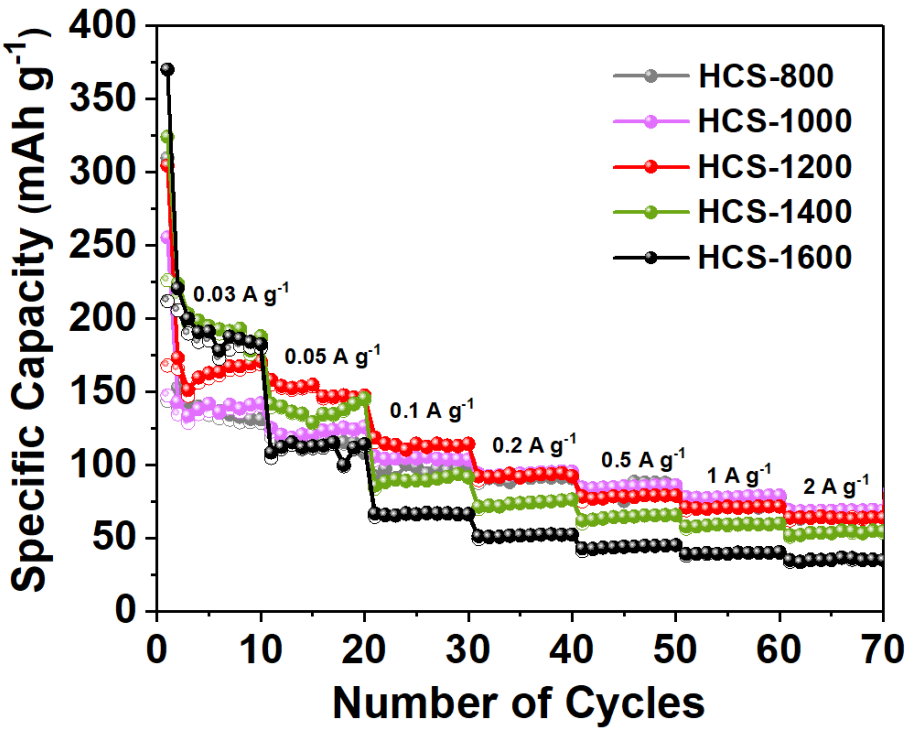

Figure S12. Rate performances of HCS-*x*.

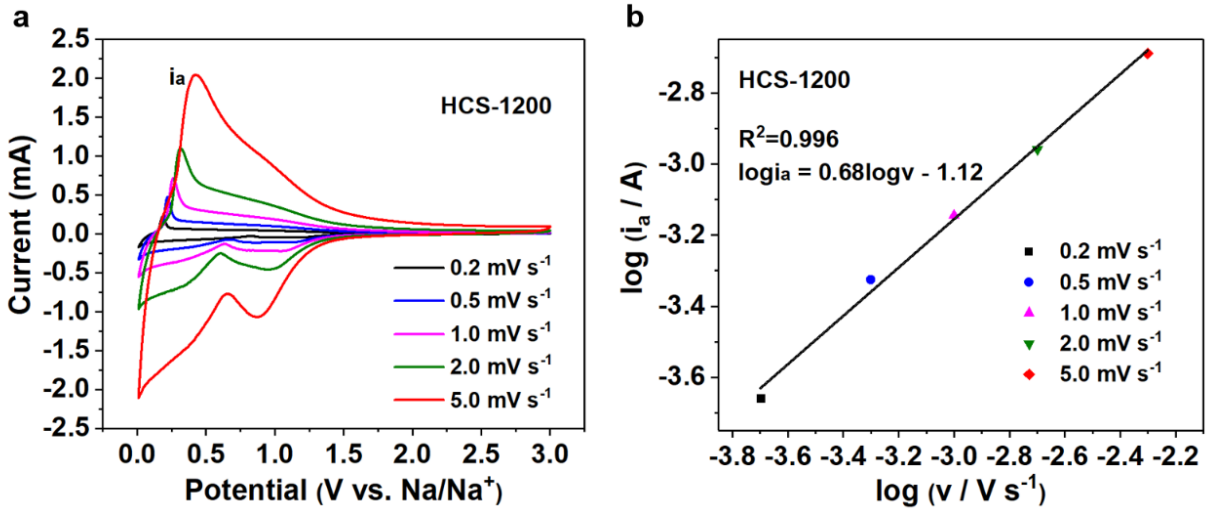

Figure S13. (a) CV curves of HCS-1200 at various scan rates. **(**b) *b*-value calculation according to the relationship between peak current and scan rate of HCS-1200.

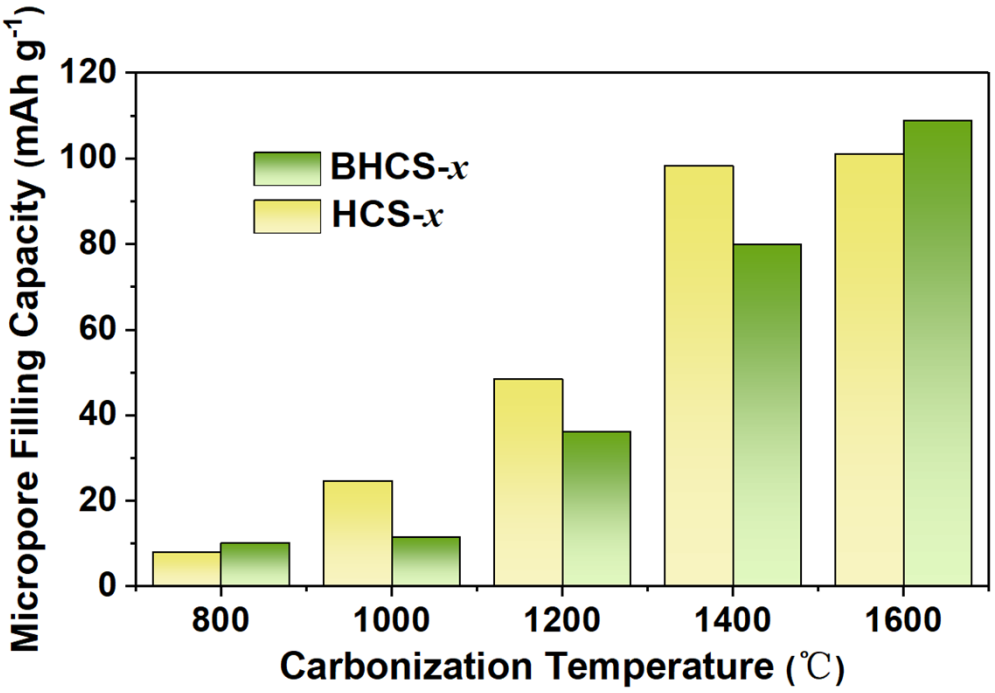

Figure S14. Capacities calculated from the micropore filling (＜0.03V) in the 2nd cycle of HCS-*x* and BHCS-*x*.

Table S3. HOMO, LUMO and band gap of carbon surface with different boron doping configurations.

	pristine carbon surface (eV)	BC_3 (eV)	BC_2O (eV)	BCO_2 (eV)
HOMO	-5.095754	-5.252507	-5.326348	-5.142229
LUMO	-2.432218	-2.86461	-2.278184	-2.444216
Gap	2.663537	2.387897	3.048163	2.698013

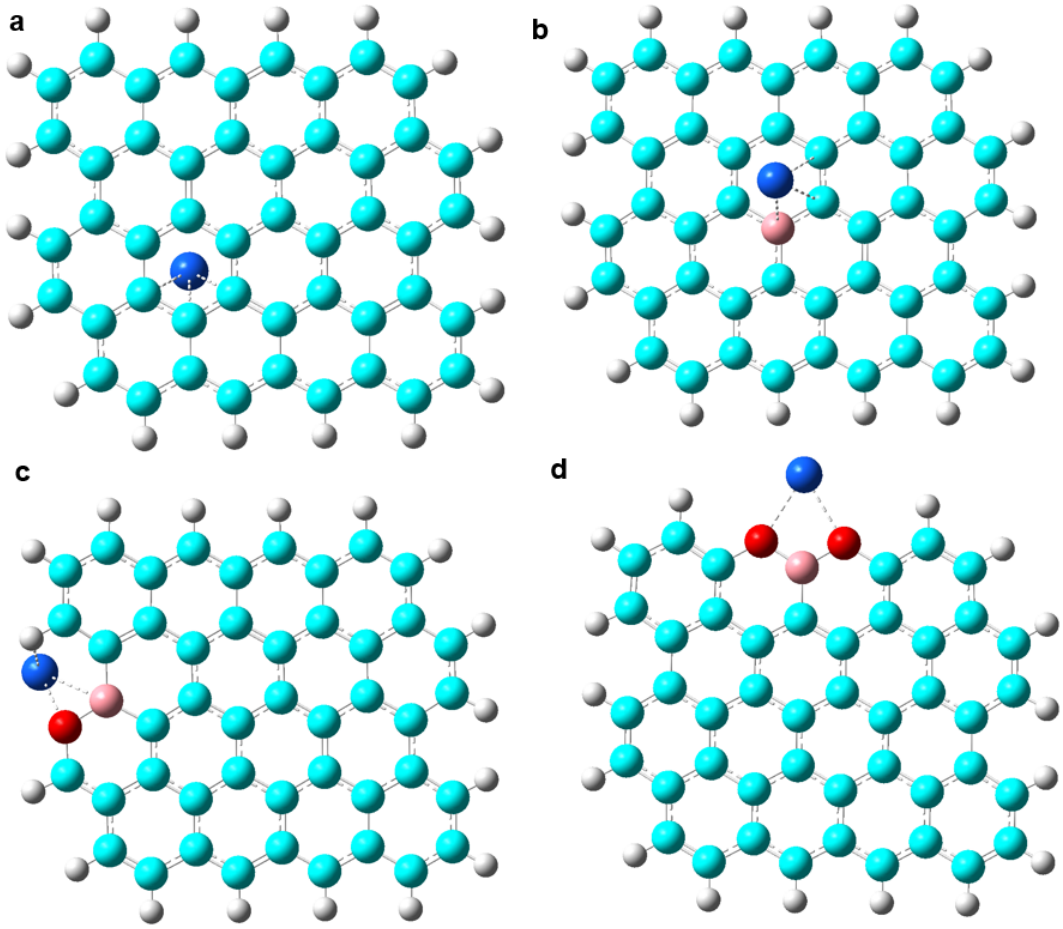

Figure S15. Na^+ adsorption configurations on various carbon surfaces.

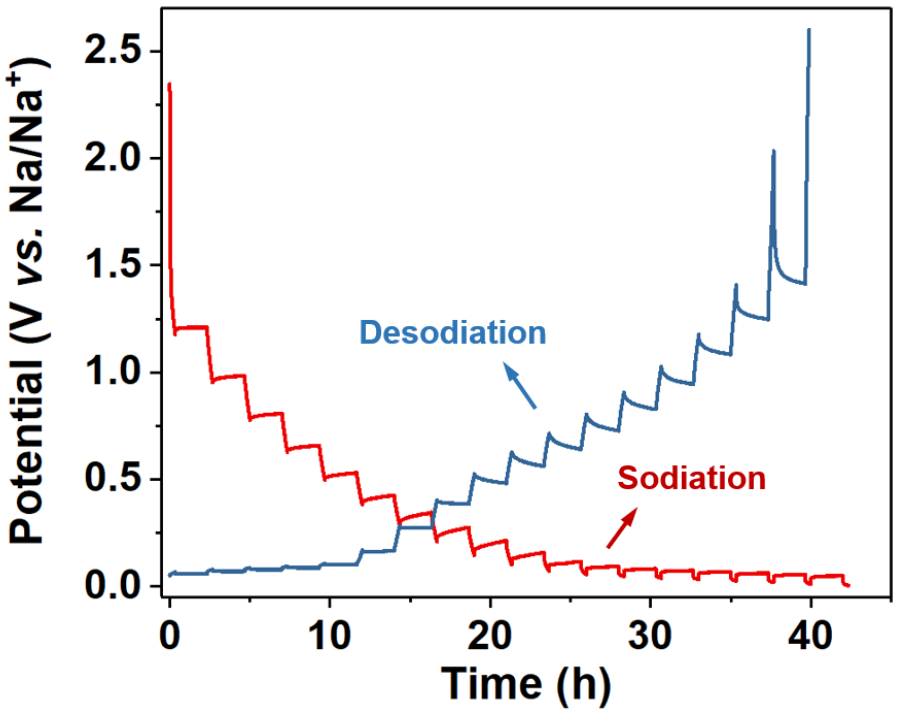

Figure S16. Galvanostatic intermittent titration technique (GITT) potential profiles of HCS-1200.

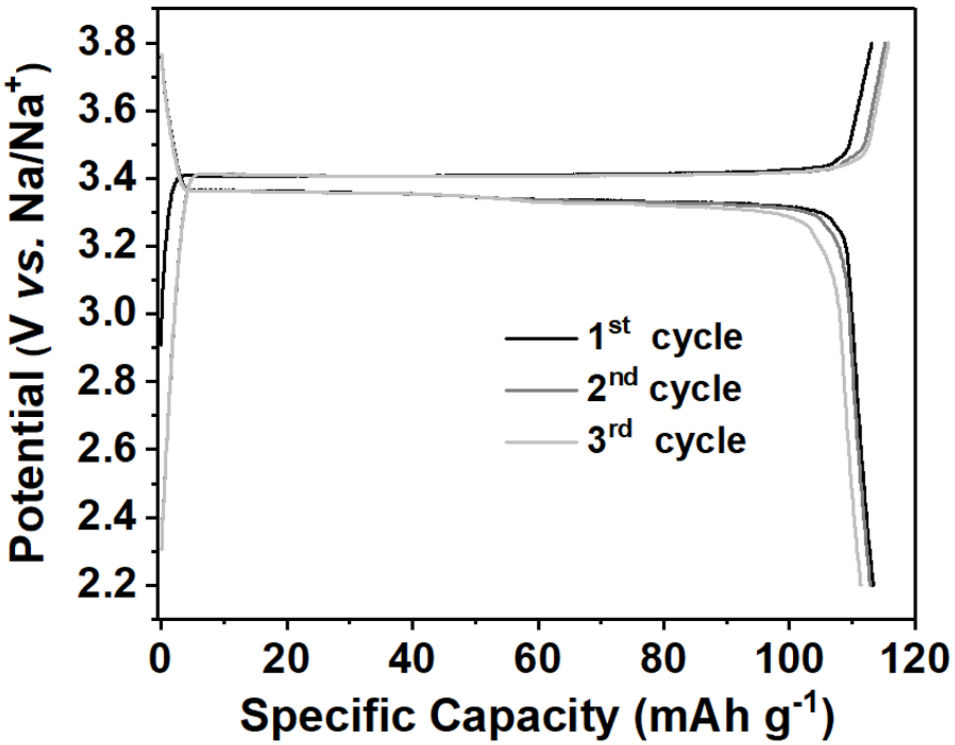

Figure S17. Initial three charge-discharge curves of NVP at the current density of 0.03 A g^{-1}

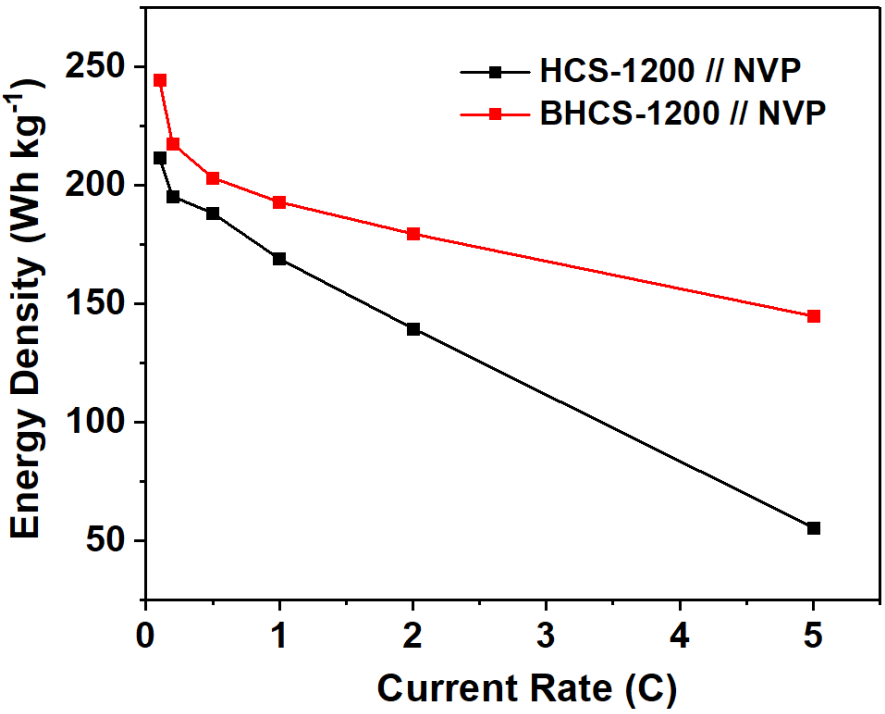

Figure S18. Energy densities of HCS-1200//NVP and BHCS-1200//NVP full-cells at different rates.